Applied Thermal Engineering 148 (2019) 1395–1406

Contents lists available at ScienceDirect

Applied Thermal Engineering

journal homepage: www.elsevier.com/locate/apthermeng

Propagation and extinction behavior of methane/air premixed flames through straight and converging-diverging microchannels

Sayan Biswas, Pei Zhang, Haifeng Wang, Li Qiao*

Purdue University, School of Aeronautics and Astronautics, West Lafayette, IN, USA

HIGHLIGHTS

- Propagation behavior of methane/air premixed flames through microchannels.
- Three propagation patterns; survival, partial extinction/re-ignition, extinction.
- Flame propagation patterns depend on channel geometry and equivalence ratio.
- Heat loss and flame stretch causes flame extinction in converging-diverging channels.

ARTICLE INFO

Keywords:
Converging-diverging (C-D) microchannels
Flame propagation
Simulations
Extinction

ABSTRACT

Propagation and extinction behavior of a CH_4/air premixed flame passing through straight and converging-diverging (C-D) microchannels (diameters ranging from 1 to 10 mm) were investigated both experimentally and numerically. The dynamic behavior of flame propagation inside the channels was experimentally studied by using CH^* chemiluminescence and direct imaging. Three patterns of flame propagation were observed, *i.e.*, the flame can survive, partially extinguish and then re-ignite downstream, or completely extinguish. Regime diagrams showing these different patterns as functions of channel geometry and equivalence ratio were generated for both the straight and C-D channels. Numerical simulations were carried out to explain the experimentally observed flame dynamics inside the channels using detailed CH_4/air chemistry. In general, flames were easier to extinguish in C-D channels than in straight channels for a fixed channel diameter and equivalence ratio. Additionally, flames were harder to survive in C-D channels with larger exit-to-throat area ratios. Both heat loss and flame stretch were key factors that can generally cause flame extinction in narrow C-D channels. Heat loss was found to be the primary reason for flame extinction inside the microchannel in comparison with the stretch effect.

1. Introduction

Combustion at small scales (micro and mesoscales) is gaining increasing attention these days due to the wide spectrum of potential applications in sensors, actuators, portable electronic devices, rovers, robots, unmanned air vehicles, thrusters, industrial heating devices, and furthermore, heat and mechanical backup power sources for air-conditioning equipment in hybrid vehicles, direct ignition (DI) engines as well [1–3]. Combustion of hydrocarbon fuels is more attractive to manufacturers of miniature power devices because the energy density of hydrocarbons is several times higher than modern batteries [4]. Microscale combustion physics is quite different from those at larger length scales. For example, flame propagation through narrow channels has unique characteristics, *e.g.*, the increasing effects of flame–wall interaction and molecular diffusion [5–9]. In small-scale combustion systems, the surface-to-volume (S/V) ratio is large, which leads to more heat loss and thus causes flame extinction more easily.

The present investigation of flame propagation through microchannels was motivated by the previous work on ignition of ultra-lean mixtures by using a turbulent hot jet [10–17]. Pre-chamber hot jet ignition has been used for heavy-duty natural gas engines, as well as in pulse detonation engines, where a small-diameter orifice (or nozzle) is used to connect a pre-chamber with the main combustion chamber. Depending on the characteristics of the hot jet issued from the pre-chamber, either a *flame jet* (if the pre-chamber flame survives heat loss and high stretch when passing the orifice) or a *hot jet* containing the combustion products only (if the pre-chamber flame extinguishes when passing the orifice) can ignite the main chamber [10–13]. The

* Corresponding author.
E-mail address: lqiao@purdue.edu (L. Qiao).

https://doi.org/10.1016/j.applthermaleng.2018.07.049
Received 18 April 2018; Received in revised form 9 July 2018; Accepted 9 July 2018
Available online 10 July 2018
1359-4311/

characteristics of the jet issuing from the pre-chamber depend on the pre-chamber initial conditions and the nozzle geometry such as nozzle length, diameter, and length to diameter (L/D) ratio. If the pre-chamber flame survives heat loss and high stretch rate inside the nozzle, a flame-jet comes out. Otherwise, the pre-chamber flame extinguishes inside the nozzle, and a hot jet containing only combustion products comes out to ignite the main chamber mixture. These two fundamentally different ignition mechanisms motivated the authors to investigate how flame propagates through microchannels. The key question is – will the flame survive or extinguish while passing through a C-D nozzle? Thus, studying the flame dynamics through C-D microchannels is of great importance for the understanding of mechanisms of turbulent hot jet ignition by using C-D nozzles. The nozzles used in practical natural gas engines have diameters ranging from 0.5 to 2 mm. Nevertheless, the term "microscale combustion" is often used when the characteristic length scale is on the same order as the "quenching distance" which is typically a few millimeters [5,18]. Since most of the channel diameters are within 1–4 mm in the present study, we have used the term "microchannel" throughout this paper.

Previous experimental, computational and theoretical work have revealed the rich physics of micro and mesoscale flame propagation. Many interesting phenomena have been observed, such as flame bifurcation, dynamic oscillating flame, and spinning flames [19–24]. Nevertheless, to the authors' knowledge, near all previous studies on flame propagation in narrow channels were focused on straight channels or slightly curved channels [25–27]. Very few have examined converging-diverging (C-D) channels [28]. In a recent study by Biswas and Qiao [11,13], it was found that using supersonic hot jets generated by using C-D nozzles can ignite leaner mixtures in the pre-chamber hot jet ignition system, leading to ultra-low emissions and higher combustion efficiency. Thus, it is important to explore the flame propagation behavior through C-D channel. The main purpose of this paper was to conduct this study of flame dynamics through C-D microchannels. Straight microchannels will also be used for comparative studies.

Furthermore, the knowledge obtained from in this study is not just limited to turbulent jet ignition. C-D microchannel flame propagation has vast wide-spread potential in areas such as micro-air propulsion systems, flow actuators, portable electronic devices, rovers, robots, unmanned air vehicles, thrusters, industrial heating devices. Thus, the context and the findings of the present work carries key information.

An experiment was developed to study CH_4/air premixed flames passing through straight and C-D microchannels. The primary goal was to find out whether the flame can survive or extinguish while passing through the channels. The influences of the equivalence ratio and channel geometry were studied. Dynamic behavior of flame propagation inside the channels was determined using direct imaging and high-speed CH* chemiluminescence, where flame shape, propagation speed, cyclic oscillatory motions, and local extinction behavior were observed. Numerical simulations of the flames passing through the microchannels were also performed, and the results were used to explain the experimental observations and to help identify flame extinction mechanisms.

2. Experimental methods and numerical models

2.1. Experimental methods

The schematic of the experimental setup is shown in Fig. 1(a) and (b). Two identical cubic-shaped carbon steel chambers (3″×3″×3″) were connected by a transparent cylindrical quartz micro-tube (type GE124, 86% UV transparent) of 10 cm length. The internal diameter, d of the quartz tubes/channels was varied from 1 mm to 10 mm. A section view of the C-D channel is shown in Fig. 1(c). The channel dimensions (channel diameter, d, channel length, L, and throat diameter, d_t for C-D channels) are listed in Table 1. For each channel diameter, both a straight channel and a C-D channel were tested. For the C-D channels, two different exit-to-throat area ratios (AR) of 4 and 9 were used. The motivation of the current study was to explore the C-D nozzle behavior to better understand the hot jet characteristics for turbulent jet ignition. Our previous study [13] showed that for AR 4 and 9, the hot supersonic jet was able to extend the lean flammability limit of premixed hydrogen/air. Thus, to explore the effect of flame behavior in a C-D microchannel, we focus on these two AR values 4 and 9.

A better view of the combustion chamber and the microchannel are shown in Fig. 1(b)–(d). The combustion chamber on the left-hand side of Fig. 1(b), which mimics a pre-chamber in gas engines with a turbulent jet ignition system, was used to generate a stably propagating laminar flame entering the microchannel. The CH_4/air mixture in the combustion chamber was ignited by using an electric spark created by a 0–40 kV capacitor discharge ignition (CDI) system. The inlet of the microchannels had a bell-shaped opening to accommodate smooth entrance of the flame. The cubic-shaped chamber on the right-side was the settling chamber, which was filled with inert gasses and served to release pressure after combustion. A ball valve located at the entrance of the settling chamber was closed during the experiment. Thus, the combustion chamber and the microchannel essentially formed a constant volume system.

High-speed CH^* chemiluminescence, high-speed direct luminosity imaging, and infrared imaging were used to visualize flame propagation in the combustion chamber and the microchannel. A high-speed camera (Vision Research Phantom v7.1), along with video-scope gated image intensifier (VS4-1845HS) with 105 mm UV lens, were utilized to detect CH^* signals at a narrow band 431 ± 12 nm detection limit. The intensifier was externally synced with the camera via a high-speed relay and acquired images at the same frame rate (up to 16,000 fps) with the Phantom camera. The pressure of the combustion chamber and the pressure at the microchannel exit were recorded using high resolution (~10 kHz) Kulite (XTEL-190) pressure transducers combined with NI-9237 signal conditioning and pressure acquisition module via the LabVIEW software.

2.2. Numerical models

To complement the experimental studies of the dynamics and extinction mechanisms of flames passing through the microchannels, we numerically simulated the transient combustion process inside the combustion chamber and the microchannel. The computational domain is shown in Fig. 2. A number of assumptions and simplifications were introduced in the simulations for simplicity and for a reduced computational cost. Since the focus of the study was mainly on the flame dynamics inside the microchannels, the simulation in the combustion chamber (as shown in Fig. 1) was simplified into a two-dimensional axisymmetric simulation by transforming the cubic combustion chamber into a cylinder with the same volume. This simplification significantly reduced the computational cost while having a negligible effect on the flame propagation along the centerline inside the combustion chamber. Such a negligible effect was confirmed by the accurate prediction of the flame propagation along the centerline inside the combustion chamber in comparison with the experimental data as will be discussed in Figs. 3 and 4. Only laminar flames were considered in the simulations. The experiments did show a possible transition of a laminar flame to a turbulent flame when a large channel diameter $d = 10$ mm was used (see Section 3.2). Laminar-to-turbulence transition was generally very challenging for the numerical modeling, and hence we did not attempt its modeling. Instead, we focused only on the laminar cases in the simulations and relied solely on the experiment to study the transitioning flames. We have neglected the effect of gravity in the numerical simulation since from the experiments we observed that there is little asymmetric behavior of the flame front. With the above simplifications and assumptions, the governing equations for the flame propagation in the 2D axisymmetric cylindrical coordinate are listed in Table 2.

In the above equations, (x, r) represent the axial and radial locations

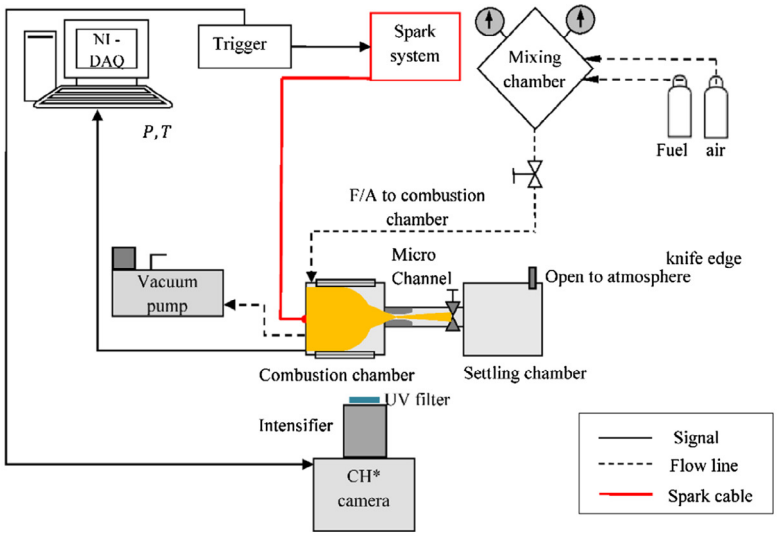

(a)

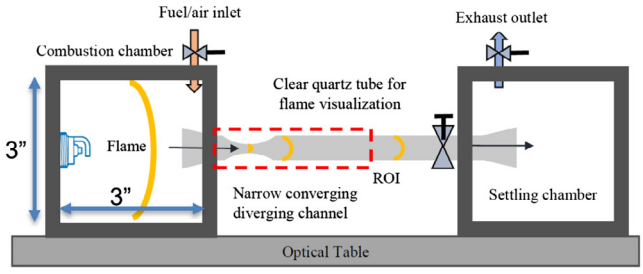

(b)

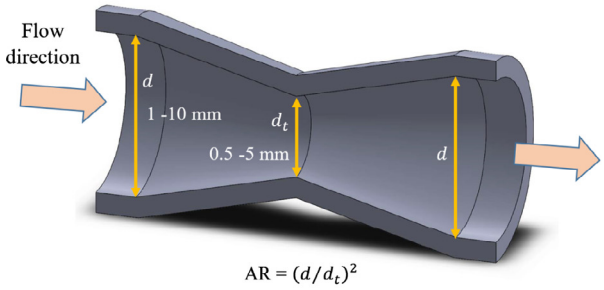

(c)

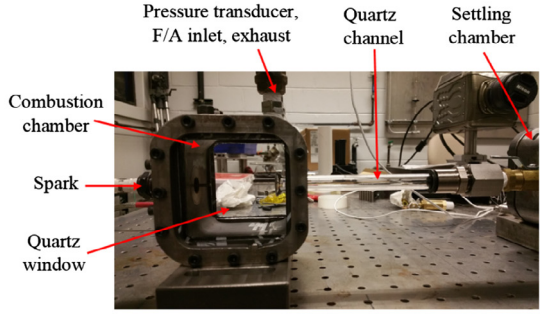

(d)

Fig. 1. (a) Schematic of the experimental setup for flame propagation through the C-D microchannel, (b) the combustion chamber and the settling chamber, (c) section view of the C-D channel, (d) image of the combustion chamber and microchannel assembly.

Table 1
Dimensions of the microchannel.

Channel #	d(mm)	L(cm)	d_t(mm)	Area ratio (AR)
1	1	10	0.5	4, 9
2	2	10	1	4, 9
3	3	10	1.5	4, 9
4	4	10	2	4, 9
5	6	10	2	4, 9
6	10	10	5	4, 9

in the 2D cylindrical coordinate, v_x and v_r are the axial and radial velocity components, respectively, ρ is density, P is pressure, T is temperature, ϕ_j is the mass fraction of the jth species, and E is the total energy. The total energy is defined as $E = h - \frac{p}{\rho} + \frac{\vec{v}^2}{2}$ and sensible enthalpy is $h = \sum_j \phi_j h_j$ with $h_j = \int_{T_{ref}}^{T} c_{p,j} dT$ and $T_{ref} = 298.15$K. The term $\nabla\cdot\left(-\sum_j h_j \vec{J_j}\right) = \sum_j \left[\frac{\partial}{\partial x}\left(h_j \rho \Gamma_j \frac{\partial \phi_j}{\partial x}\right) + \frac{1}{r}\frac{\partial}{\partial r}\left(r h_j \rho \Gamma_j \frac{\partial \phi_j}{\partial r}\right)\right]$ in Eq. (5) is the energy change due to species diffusion and the term $\nabla\cdot(\bar{\bar{\tau}}\cdot\vec{v})$ is the energy dissipation term where $\bar{\bar{\tau}}$ is the stress tensor. The transport properties in the equations include the dynamic viscosity μ, molecular diffusivity Γ_j, and thermal conductivity k. The Eqs. (1)–(6) are solved using the ANSYS Fluent 17.1 with the pressure-based solver. For more details about the numerical methods, the readers are referred to the

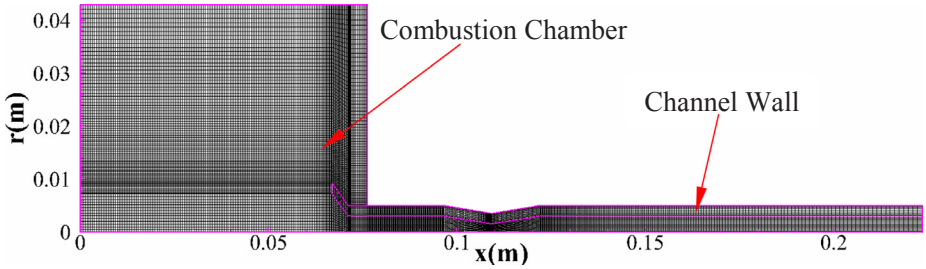

Fig. 2. The computational domain and the mesh for the microchannel flames with conjugate heat transfer.

Fluent User's Guide.

The employed computational domain and mesh are shown in Fig. 2. A non-uniform mesh was used which had a high grid resolution (Δx = 0.072~0.2 mm) around the C-D nozzle and was stretched to the combustion chamber (Δx = 0.24 mm) and to the end of the microchannel (Δx = 0.63 mm). In total, the computational mesh consisted of n_{cell} = 128, 179 grid cells for the simulation results presented in the paper. The grid convergence is examined later in Fig. 3. In the area of main interest near the C-D nozzles, there were about 10 grid cells inside the flame to resolve the flame front. The time step size used in the simulations was $\Delta t = 10^{-5}$ s which was chosen to balance the computational cost and the accuracy to capture the premixed flame propagation.

The heat loss from the microchannels was generally expected to have a significant effect on the microchannel flame propagation and extinction because of the relatively large surface-area/volume ratio in small scale. Such an effect was difficult to examine by using the current experiments. Thus we relied on the simulations to help examine the effect of heat loss on the flame propagation. To do so, we used in the simulations two different thermal boundary conditions to the walls of the microchannels, an adiabatic condition or a conjugate heat transfer. In the conjugate heat transfer simulations, the following physical properties for the microchannel wall (fused quartz) were used: density 2200 kg/m^3, thermal conductivity 1.38 W/m·K, and specific heat 740 J/kg·K). The wall thickness is specified according to the experiment to be δ = 1.5 mm for the microchannels of diameters d = 1 mm and d = 3 mm and δ = 2 mm for the other microchannels. The convection heat transfer coefficient on the outer surface of the channel wall was estimated to be 10 W/m^2-K based on a natural convection heat transfer surrounding a cylinder [29], for imposing the thermal boundary condition for the conjugate heat transfer analysis.

To ignite the flame in the simulations, we placed an initial hot spot of 3 mm in diameter at the location (x, r) = (3 mm, 0 mm) to mimic a spark flame ignition. The chemical mechanism for CH_4 oxidation was described by GRI-Mech 1.2 [30,31] which had 32 species and 175 reactions. *In situ* adaptive tabulation (ISAT) [32] was used to accelerate the numerical integration of chemical reactions with an error tolerance 10^{-4}. Second order accurate numerical schemes were chosen for the temporal and spatial discretization in the numerical simulations.

To confirm the adequacy of the used grid resolution, a grid convergence test is done for the case with a straight microchannel with the diameter d = 4mm and the equivalence ratio ϕ = 0.9. The convergence results are reported in Fig. 3. Five different grids were used with n_{cell} = 31, 175, 71,224, 128,179 (current), 200,234, and 291,023. In the left subplot of Fig. 3, the profiles of the flame tip displacement speed against the centerline flame displacement are shown. The displacement speed is nearly constant around 1.9 m/s at the initial stage, decreases when the flame is getting closer to the channel entrance, and has a sudden increase after the flame enters the channel. The result with the current grid (n_{cell} = 128, 179) shown by the blue dash-dot line with diamonds shows reasonable grid independence with the maximum error of about 10% relative to the finest grid result with n_{cell} = 291, 023. The second-order grid convergence is confirmed in the right subplot of Fig. 3 where the flame tip displacement speeds at selected flame tip displacement locations (30 mm, 50 mm, 60 mm and 70 mm) are shown against $1/n_{cell}$. The linear convergence behavior of the simulation results against $1/n_{cell}$ (excluding the coarsest grid results) indicates the second-order grid convergence since the grid size is proportional to $1/\sqrt{n_{cell}}$. The observed second-order convergence is consistent with the order of accuracy of the employed numerical methods and hence verifies the current numerical simulations. The specified grid with n_{cell} = 128, 179 for all the following numerical studies is found to be able to yield a reasonably accurate flame tip displacement speed with a feasible computational cost.

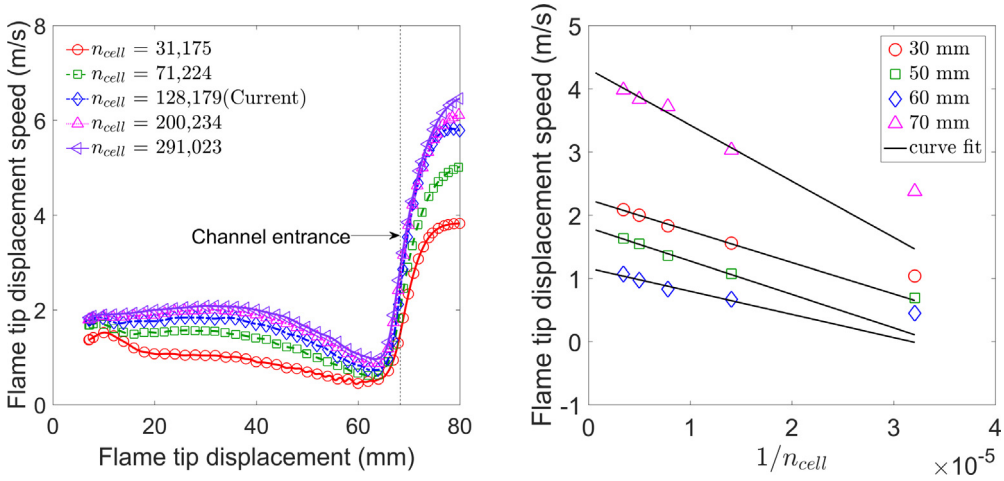

Fig. 3. Grid convergence study of the predicted flame displacement speeds with different grid resolutions n_{cell} in a straight microchannel with d = 4mm and ϕ = 0.9.

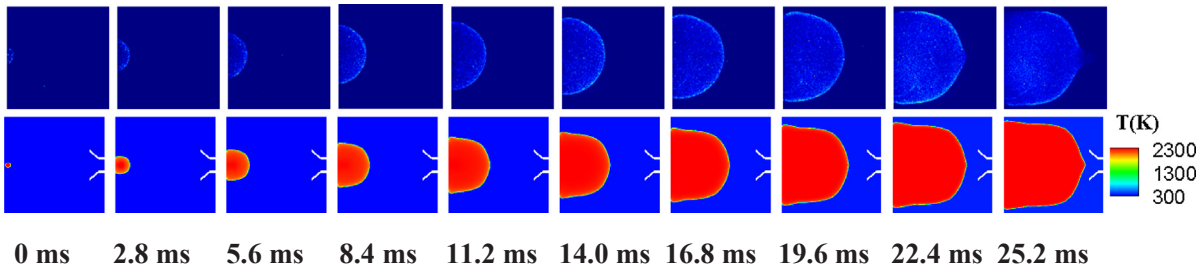

Fig. 4. High-speed CH* chemiluminescence images of flame propagation (top) and numerically simulated temperature contour (bottom) in the combustion chamber.

3. Results and discussion

3.1. Flame propagation in the combustion chamber

We first examined the flame behavior in the combustion chamber before it entered the microchannel. The CH* chemiluminescence images of flame propagation in the combustion chamber are shown in Fig. 4 (top), and the simulated flame temperature contours are shown on the bottom of Fig. 4. As the spark, which was located on the center-left side of the chamber, ignited the premixed CH_4/air, a hemispherical shaped laminar flame was observed to propagate outwardly. Since CH* is generated on the flame front where heat release is maximum, the strongest signals indicate the location of the flame front. As the flame approached near the entrance of the microchannel, the flame tip converted into an elongated-shaped flame front. The simulation captured the flame front indicated by the temperature contour reasonably well. Slight difference in the predicted flame front curvature from the measurement is expected to be caused by the simplified 2D simulations discussed in Section 2.2.

Fig. 5 compares the time history of the measured and simulated flame tip displacement for three equivalence ratios. After the initial transient of spark ignition, the flame propagated nearly at a constant speed (laminar flame speed) inside the chamber, as indicated by the straight lines in the displacement-versus-time diagram for a time less than 30 ms. The slope of the displacement-versus-time diagram is higher for $\phi = 1.0$ than $\phi = 0.9$ and 0.8. This is expected since the laminar flame speed is maximum near stoichiometric condition. As the flame entered the microchannel, however, the flame tip velocity increased rapidly indicated by the curves above the "channel entrance" line. This acceleration was caused by high-pressure combustion products pushing the unburned fuel/air mixture through the smaller diameter channel. The simulations accurately reproduced the measurements of the flame tip displacement inside the combustion chamber, which confirms the minor effect of using simplified 2D simulations for the combustion chamber.

3.2. Flame dynamics in microchannels

Once the flame enters the microchannel, depending on the channel geometry and the equivalence ratio, the flame dynamics vary. Fig. 6(a)–(f) compares the time sequence of CH* chemiluminescence images of flame propagation process through straight and C-D channels with internal diameter, $d = 10$ mm, 2 mm, and 1 mm, respectively.

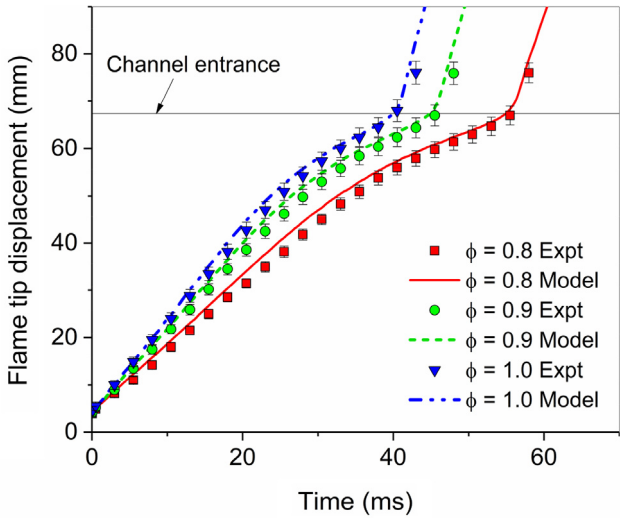

Fig. 5. Measured and simulated time history of flame tip displacement through $d = 10mm$ for $\phi = 0.8$, 0.9, and 1.0.

Fig. 6(a) shows flame propagation through a 10 mm straight channel. The finger-shaped flame front steadily passed through the channel. However, in the C-D channel of the same inlet diameter and with AR = 4, as seen in Fig. 6(b), the flame became unstable after passing through the throat. The hemispherical shape of the flame front vanished, and the flame became turbulent as evident from the CH* emission. As a result of turbulent flame propagation, the time to travel through the entire channel length was shorter for the C-D channel (2.3 ms) compared to the straight channel (4.2 ms).

Flame behavior changed with a decrease in channel diameter. Fig. 6(c) and (d) presents flame propagation under the stoichiometric condition ($\phi = 1$) through a 2 mm microchannel – both straight and C-D. The flames became weaker, as evident from the weaker CH* signals

Table 2
Governing equations used in the numerical simulation.

Continuity	$\frac{\partial \rho}{\partial t} + \frac{\partial}{\partial x}(\rho v_x) + \frac{1}{r}\frac{\partial}{\partial r}(r\rho v_r) = 0$	(1)
x-momentum	$\frac{\partial}{\partial t}(\rho v_x) + \frac{\partial}{\partial x}(\rho v_x v_x) + \frac{1}{r}\frac{\partial}{\partial r}(r\rho v_r v_x) = -\frac{\partial P}{\partial x} + \frac{\partial}{\partial x}\left[\mu\left(2\frac{\partial v_x}{\partial x} - \frac{2}{3}\left(\frac{\partial v_x}{\partial x} + \frac{1}{r}\frac{\partial r v_r}{\partial r}\right)\right)\right] + \frac{1}{r}\frac{\partial}{\partial r}\left[r\mu\left(\frac{\partial v_x}{\partial r} + \frac{\partial v_r}{\partial x}\right)\right]$	(2)
r-momentum	$\frac{\partial}{\partial t}(\rho v_r) + \frac{\partial}{\partial x}(\rho v_x v_r) + \frac{1}{r}\frac{\partial}{\partial r}(r\rho v_r v_r) = -\frac{\partial P}{\partial r} + \frac{\partial}{\partial x}\left[\mu\left(\frac{\partial v_x}{\partial r} + \frac{\partial v_r}{\partial x}\right)\right] + \frac{1}{r}\frac{\partial}{\partial r}\left[r\mu\left(2\frac{\partial v_r}{\partial r} - \frac{2}{3}\left(\frac{\partial v_x}{\partial x} + \frac{1}{r}\frac{\partial r v_r}{\partial r}\right)\right)\right] - 2\mu\frac{v_r}{r^2} + \frac{2}{3}\frac{\mu}{r}\left(\frac{\partial v_x}{\partial x} + \frac{1}{r}\frac{\partial r v_r}{\partial r}\right)$	(3)
Mass fraction of species	$\frac{\partial}{\partial t}(\rho\phi_j) + \frac{\partial}{\partial x}(\rho v_x \phi_j) + \frac{1}{r}\frac{\partial}{\partial r}(r\rho v_r \phi_j) = \frac{\partial}{\partial x}\left(\rho\Gamma_j\frac{\partial \phi_j}{\partial x}\right) + \frac{1}{r}\frac{\partial}{\partial r}\left(r\rho\Gamma_j\frac{\partial \phi_j}{\partial r}\right) + S_j,\ j = 1, 2, \cdots, N_s$	(4)
Energy	$\frac{\partial}{\partial t}(\rho E) + \frac{\partial}{\partial x}(v_x(\rho E + P)) + \frac{1}{r}\frac{\partial}{\partial r}(r v_r(\rho E + P)) = \frac{\partial}{\partial x}\left(k\frac{\partial T}{\partial x}\right) + \frac{1}{r}\frac{\partial}{\partial r}\left(rk\frac{\partial T}{\partial r}\right) + \nabla\cdot\left(-\sum_j h_j\vec{J_j} + (\bar{\bar{\tau}}\cdot\vec{v})\right) + S_h$	(5)
Equation of state	$P = \rho RT = \rho R_u T\sum_j \frac{\phi_j}{MW_j}$	(6)

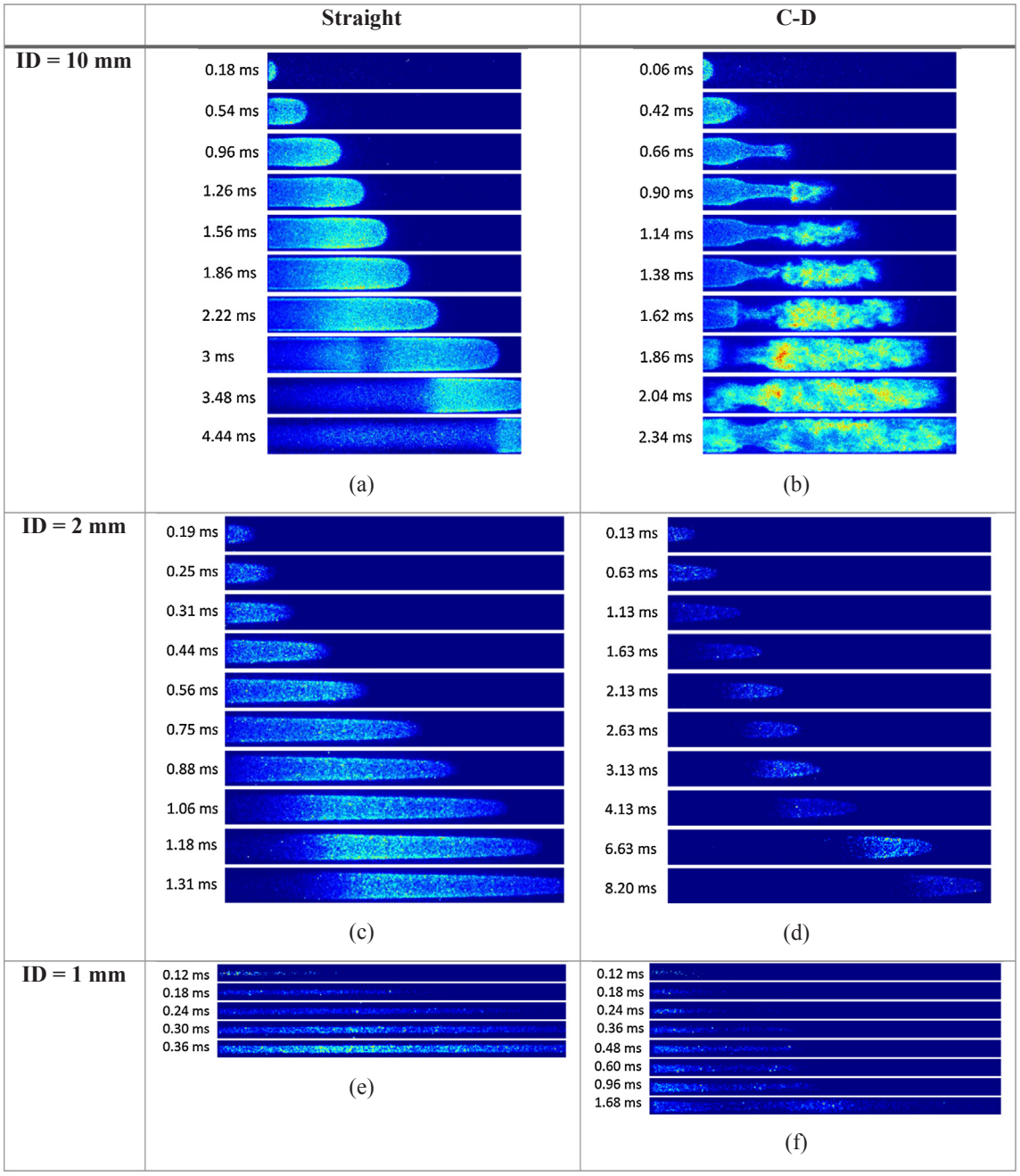

Fig. 6. The time sequence of CH^* chemiluminescence images showing flame propagation process through different diameters of straight and C-D channels with AR = 4, $\phi = 1$.

and the shorter length of the reacted (burned) zone, likely due to both increased heat loss to the channel walls and increased flame stretch. The flame remained the finger-liked shape while passing through the straight channel. After passing through the C-D section, however, the flame width shrunk, and it could not occupy the entire channel width. This could be attributed to increasing stretch due to higher velocity at the throat. Unlike the 10 mm case, the flame remained laminar after passing the throat. For straight channels, the propagation speed (location of flame front as a function of time) was nearly constant. Nevertheless, for C-D channels, the flame front location was not linear with time, especially after passing through the throat the flame slowed down.

The time sequence of flame propagation through a 1 mm microchannel is shown in Fig. 6(e) and (f). A thin, sharp-tip flame passed through the straight channel. Depending on the equivalence ratio, the flame barely passed and extinguished in most cases inside the 1 mm microchannel. The flame could not pass when $\phi < 0.9$ or $\phi > 1.2$.

Unlike the 10 mm channel, for the 2 mm (as well as the 1 mm channel), the time taken for the flame to travel through the channel length increased significantly for the C-D channel (8.2 ms) compared to the straight channel (1.3 ms). Due to the presence of the C-D section, it was expected for the flame to pass through the channel faster. This holds true for higher channel diameter (10 mm). Passing through the C-D section of the 10 mm channel, the flame became turbulent and propagated faster. For 2 mm or 1 mm channel diameter, the flame front was stretched after passing through the throat. Higher stretch slowed down the flame after it passed the throat for the 1 mm and 2 mm C-D microchannels.

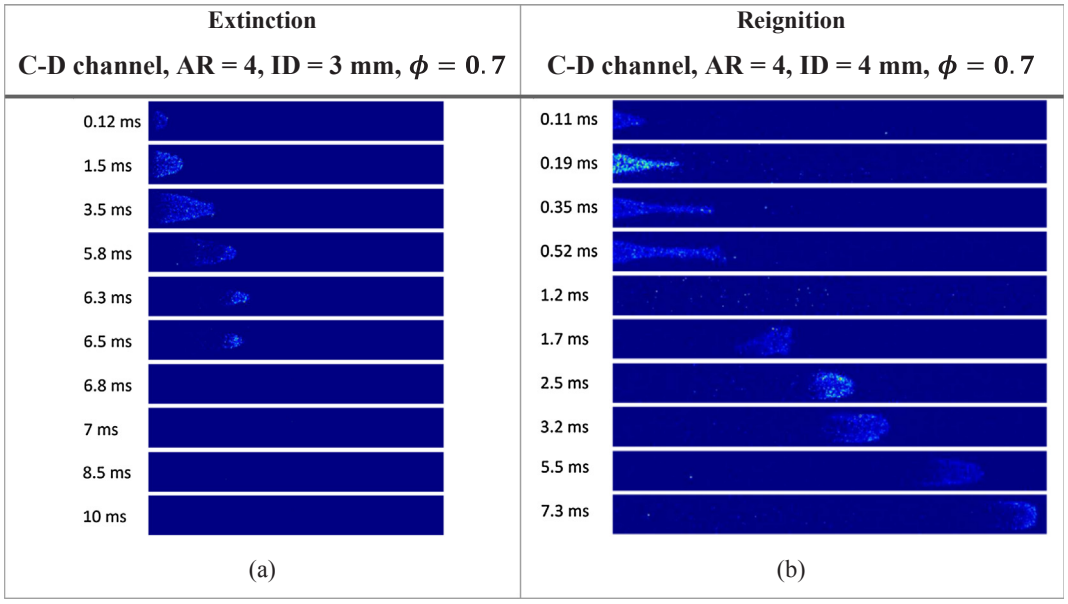

Fig. 7. The time sequence of CH^* chemiluminescence images showing flame extinction and reignition processes.

3.3. Extinction and reignition phenomena

Flame dynamics becomes interesting as we move away from the stoichiometric condition for smaller channels. Fig. 7 compares the flame propagation pattern through two C-D channels with the same aspect ratio but different diameters. The equivalence ratio for the two cases was the same. For the 3 mm C-D channel (a), the flame was extinguished after passing through the throat, likely due to heat losses and high stretch. However, for the 4 mm C-D channel (b), the flame extinguished partially just at the downstream of the throat. It was reignited again once it arrived at the straight section in the channel.

3.4. Three patterns: passing, partially passing and not passing

The flame passing behavior in the microchannels depends on the channel geometry and the equivalence ratio of CH_4/air mixtures. Fig. 8 illustrates the time history of flame tip displacement for three different geometric and mixture conditions. Numerical simulations closely match with experimental results. Based on the distinct observations whether the flame will pass, pass after retardation/oscillations (partially passing) or extinguish inside the microchannel as seen from Fig. 8, the flame behavior in the microchannel can be divided into three categories:

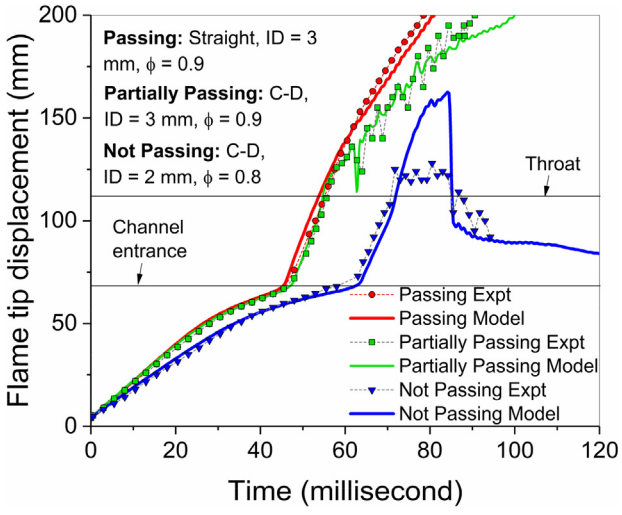

Fig. 8. Three different flame passing patterns in the C-D microchannel.

Passing: When a flame runs through the entire channel stably without any oscillations or retardation inside the channel.

Partially Passing: When a flame passes the channel after retardation or oscillations. The flame seems to stand still, oscillate or extinguish momentarily inside the channel and then reignites and passes through the channel eventually. Oscillation in the flame tip is evident from Fig. 8.

Not Passing: When the flame extinguishes in the channel and is unable to pass the entire length.

Fig. 9 summarizes the three flame passing behaviors as functions of channel diameter and equivalence ratio for straight and C-D channels with AR = 4 and 9, respectively. Overall, for both straight and C-D channels, when the equivalence ratio and channel diameter decrease, the flame pattern shifted from passing to not-passing. Additionally, a flame could pass through a straight channel more easily than a C-D channel for a given diameter and equivalence ratio. Moreover, as AR was increased from 4 to 9, the region for passing became even narrower, indicating the flame was more likely to extinguish at higher values of AR. This was because as the throat diameter decreased, the flame was exposed to higher stretch, leading to extinction more easily. The simulations with conjugate heat transfer confirmed the identification of the different passing behaviors, and this will be discussed in following sections.

3.5. Effect of heat loss

As discussed earlier, heat loss and high stretch are the two mechanisms likely responsible for flame extinction in the straight and C-D microchannels. Fundamentally, when microchannel diameter decreased, both the effects of stretch and heat loss increased to lead to potential flame extinction. In this section, we numerically examined the effect of heat loss on the flame propagation process to isolate its effect from the stretch effect during extinction. The test conditions marked by a grey-shaded box in Fig. 9(b) were selected for simulations corresponding to a C-D channel with AR = 4. Two sets of simulations were conducted, one with an adiabatic wall boundary condition and the other considering heat loss through the channel wall using conjugate heat transfer as discussed in Section 3. Fig. 10 compares the flame pattern diagram obtained from the simulations with and without heat

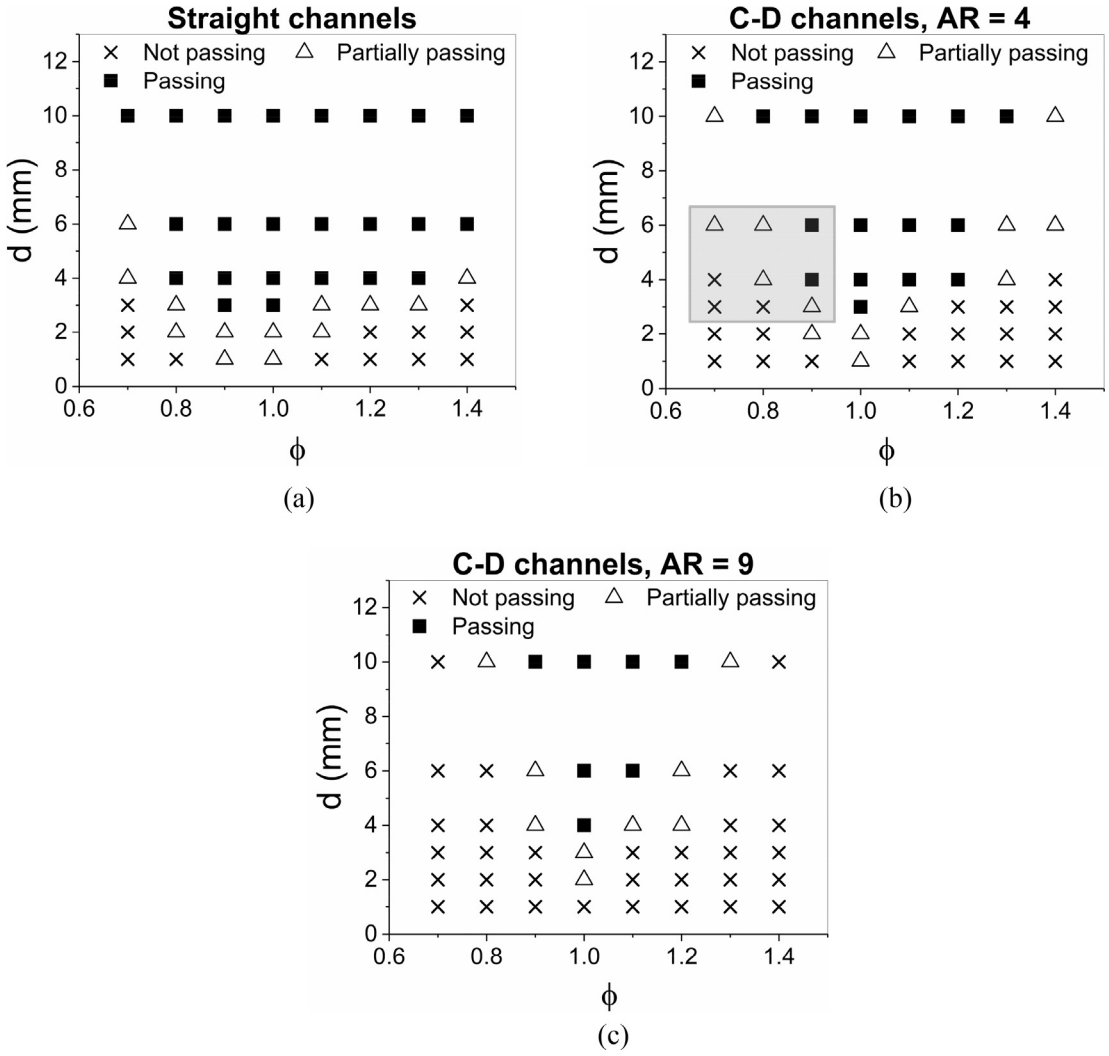

Fig. 9. Diagram of three different flame behaviors as functions of channel diameter and equivalence ratio for (a) straight channels, (b) C-D channels with AR = 4, (c) C-D channels with AR = 9, based on the experimental observations.

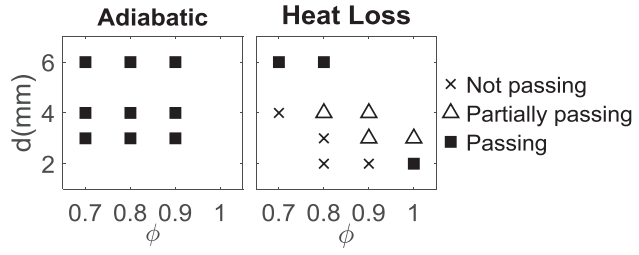

Fig. 10. Predicted flame behavior with and without heat loss.

loss. From the experimental Fig. 9(b), it was observed that the critical equivalence ratio moved toward $\phi = 1.0$ when the channel diameter decreased from 6 mm to 2 mm. Numerical modeling with conjugate heat transfer was able to predict this similar trend while the adiabatic case predicted passing for all conditions. In other words, pure stretch effect (without heat loss effect) hardly affects the flame passing behaviors in Fig. 10. This implies that heat loss was a dominant factor to cause the flame to either partially pass or not pass through the C-D microchannels.

To further illustrate the significance of heat loss, Fig. 11 shows the time sequence of predicted OH contours in the microchannel from two simulations for a C-D channel with d = 3 mm, AR = 4 and $\phi = 0.8$, with adiabatic boundary condition and with the conjugate heat transfer. For the adiabatic case, the flame passed through the channel smoothly and the mass fraction of OH was high behind the flame front. For the conjugate heat transfer case, the flame entering the channel seemed to be separated from the combustion chamber combustion products as seen from the OH contours. The annihilated OH behind the flame front in the conjugate heat transfer case was probably caused by the significant heat loss to the wall. After the throat, the flame front fluctuated for some time and eventually extinguished downstream for the conjugate heat transfer case, due to lack of weakened thermal support behind the flame front.

3.6. Effect of stretch

From Section 3.5, we were able to identify the significant effect of heat loss on flame extinction when the channel diameter was reduced. The effect of flame stretch seemed to be the secondary effect on flame extinction for study cases. In this section, we isolated the effect of stretch on the flame propagation pattern from the effect of heat loss. We compared three cases, of C-D microchannels of two different area ratios, and the other one was a straight microchannel. All the conditions such as channel diameter and ϕ were kept identical, so that the heat loss effect can be approximately fixed to isolate the effect of stretch. We expected the major difference between the two cases was the stretch rate which was higher in the C-D channel than in the straight channel.

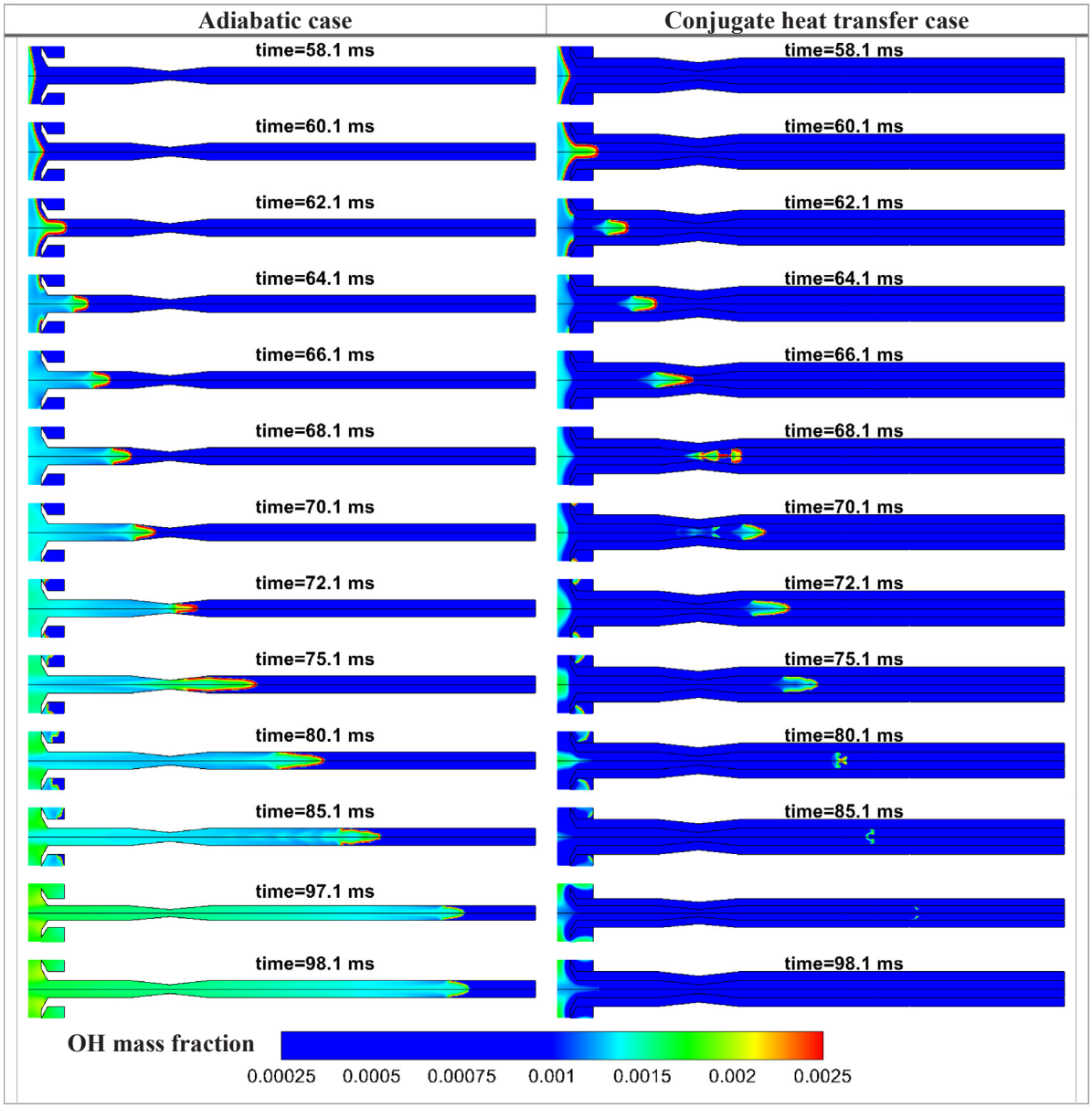

Fig. 11. The time sequence of the computed OH contours showing the effect of heat loss (C-D, ID = 3 mm, AR = 4, and $\phi = 0.8$).

From the experimental results shown in Fig. 9, it was observed that for the same channel diameter the critical equivalence ratio in the C-D microchannel was closer to the stoichiometric condition compared to the straight channel. This observation demonstrated the effect of stretch on flame propagation behaviors. Flames subjected to a higher stretch rate were more vulnerable to extinction. Similar effect of stretch was observed from the numerical simulations (results not shown). Fig. 12 compares experimentally measured flame tip velocity magnitude for two C-D channels with area ratio 4 and 9 and a straight channel with the same internal diameter, d = 3 mm and equivalence ratio, $\phi = 0.8$. Since the stretch rate is proportional to the velocity gradient, the flame tip velocity provided a qualitative measure of the effect of stretch. The flame tip velocity oscillations in the C-D channels were much higher compared to the straight channel. Among two different area ratios, AR = 9 had higher velocity oscillations. Hence, the flame in C-D channel of AR = 9 was more susceptible to higher stretch rate. Oscillating flame in microchannel had been observed by several researchers [33,34]. Flame oscillation behavior in microchannel could be attributed to the competition between wall heat loss and heat gain from upstream combustion. Flame shrunk after losing heat through the wall. As the flame shrunk the effect of heat loss diminished and the flame could be stabilized by enhanced burning rate. This periodic behavior continued until the flame could not withstand the stretch or if it experienced excessive heat loss.

The experimental observations motivated the authors to construct a stable flame passing criteria using the flame tip velocity near C-D channel information presented in Section 3.4. Fig. 13 plots the outcomes of the flames on the flame tip velocity vs. equivalence ratio diagram. As evident from Fig. 13(a), stable flame propagation limit is a strong function of the equivalence ratio. A stoichiometric flame with a flame tip velocity of 35 m/s can stably pass through the channel. As the equivalence ratio goes down, the critical flame tip velocity to sustain a stable flame goes down as well. There exists a triangular region on this velocity versus equivalence ratio diagram, within which stable flame propagation is possible. Fig. 13(b) presents the stable flame propagation criteria for the C-D channel. At first glance, it might seem that the size of the stable flame propagation zone decreases for C-D channels. However, the flame can withstand a greater velocity in the C-D channel. As an example, when the stable passing limit in a straight channel is 35 m/s for $\phi = 1$, it is 46 m/s for a C-D channel.

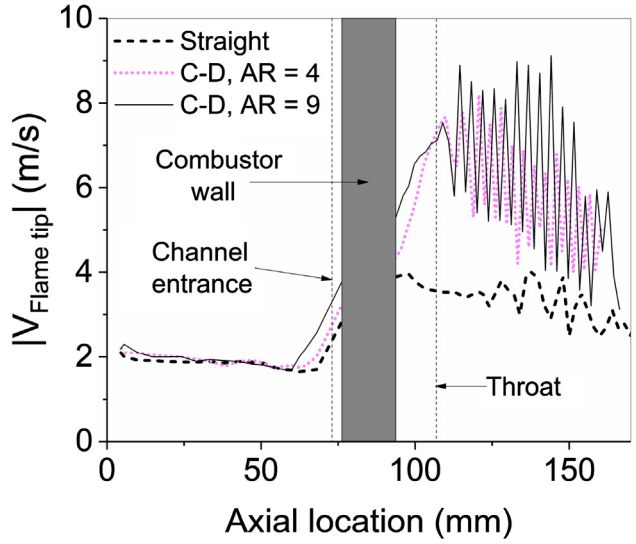

Fig. 12. Flame tip velocity in C-D channels and straight channel for ID = 2 mm, $\phi = 0.8$.

However, Fig. 13 has an inherent drawback. It is dependent upon channel diameter. To remove this dependency on channel diameter, we plotted the strain rate in Fig. 14. The strain rate tensor for a fluid with velocity u can be expressed as,

$$\epsilon_{ij} = \frac{1}{2}\left(\frac{\partial u_i}{\partial x_j} + \frac{\partial u_j}{\partial u_i}\right) = \frac{1}{2}\left(\frac{\partial u}{\partial y} + \frac{\partial u}{\partial x}\right) \tag{7}$$

We can safely assume there is no velocity gradient in the x-direction. Thus, $\partial u/\partial x = 0$. Thus, strain rate can be expressed as,

$$\epsilon = \frac{1}{2}\frac{\partial u}{\partial y} = \frac{U_C}{d} \tag{8}$$

where U_c is centerline velocity of microchannel and d is channel diameter.

Fig. 14(a) and (b) shows that flame in the C-D channel can withstand slightly more strain near the stoichiometric condition. In off-stoichiometric condition, both straight and C-D channel flames undergo similar strain rates. However, for lower equivalence ratio, in C-D channel even at a lower strain rate, flame could not pass through the channel. Fig. 14(c) shows the strain rate as a function of equivalence ratio for AR = 9. The maximum strain rate at the stoichiometric condition for a higher area ratio, AR = 9, C-D channel is nearly same with AR = 4. But the key observation is the shrinkage of the flame passing zone. At lower equivalence ratio, the flame becomes extremely susceptible to any strain rate imposed on it. Thus, at lower equivalence ratio even for a much lower strain rate than maximum strain imposed on $\phi = 1$, the flame was unable to pass through the C-D channel.

From Sections 3.5 and 3.6, we were able to isolate the effect of stretch from heat losses to characterize flame extinction behavior inside the microchannels. Comparing the effects of heat loss and stretch in the microchannel flames, heat loss had a more noteworthy influence on flame extinction, as discussed in Section 3.5.

4. Conclusions

This paper describes the dynamics of premixed CH_4/air flame propagation through straight and C-D microchannels. The key findings are summarized below.

1. While a finger-shaped flame passed through the straight channel, the shape of the flame passing through the C-D channels changed with the diameter. For a higher channel diameter, the flame became turbulent passing through the divergent section. For a smaller diameter channel, the flame remained laminar and was likely to extinguish near the throat and was reignited at the downstream.
2. Three flame behaviors were observed – passing, partially passing, and extinguish, depending on the channel geometry and equivalence ratio. In general, flames were easier to extinguish in C-D channels than in straight channels for a fixed channel diameter and equivalence ratio. Additionally, flames were harder to survive in C-D channels with larger exit-to-throat area ratio (higher contraction).
3. Both heat loss and flame stretch were factors that could cause flame extinction in small C-D channels. Simulations with and without heat

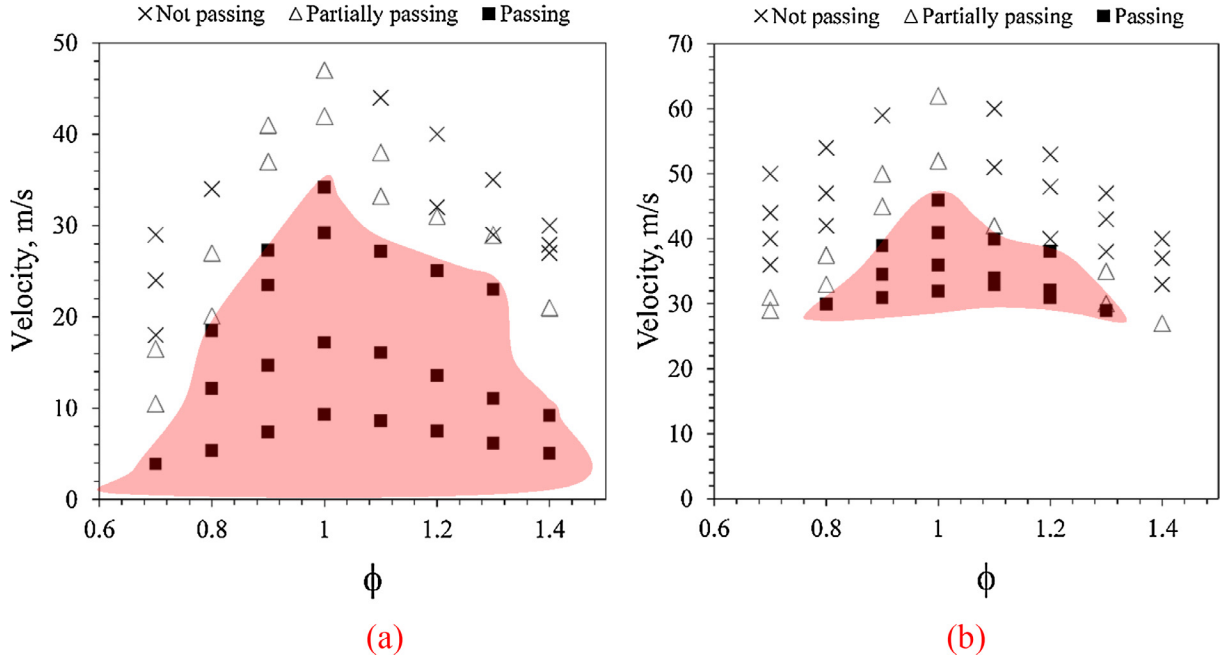

Fig. 13. Stable flame propagation limit (marked by colored zone) through (a) straight channels and (b) C-D channels on a flame tip velocity (near C-D throat entrance) versus equivalence ratio plot.

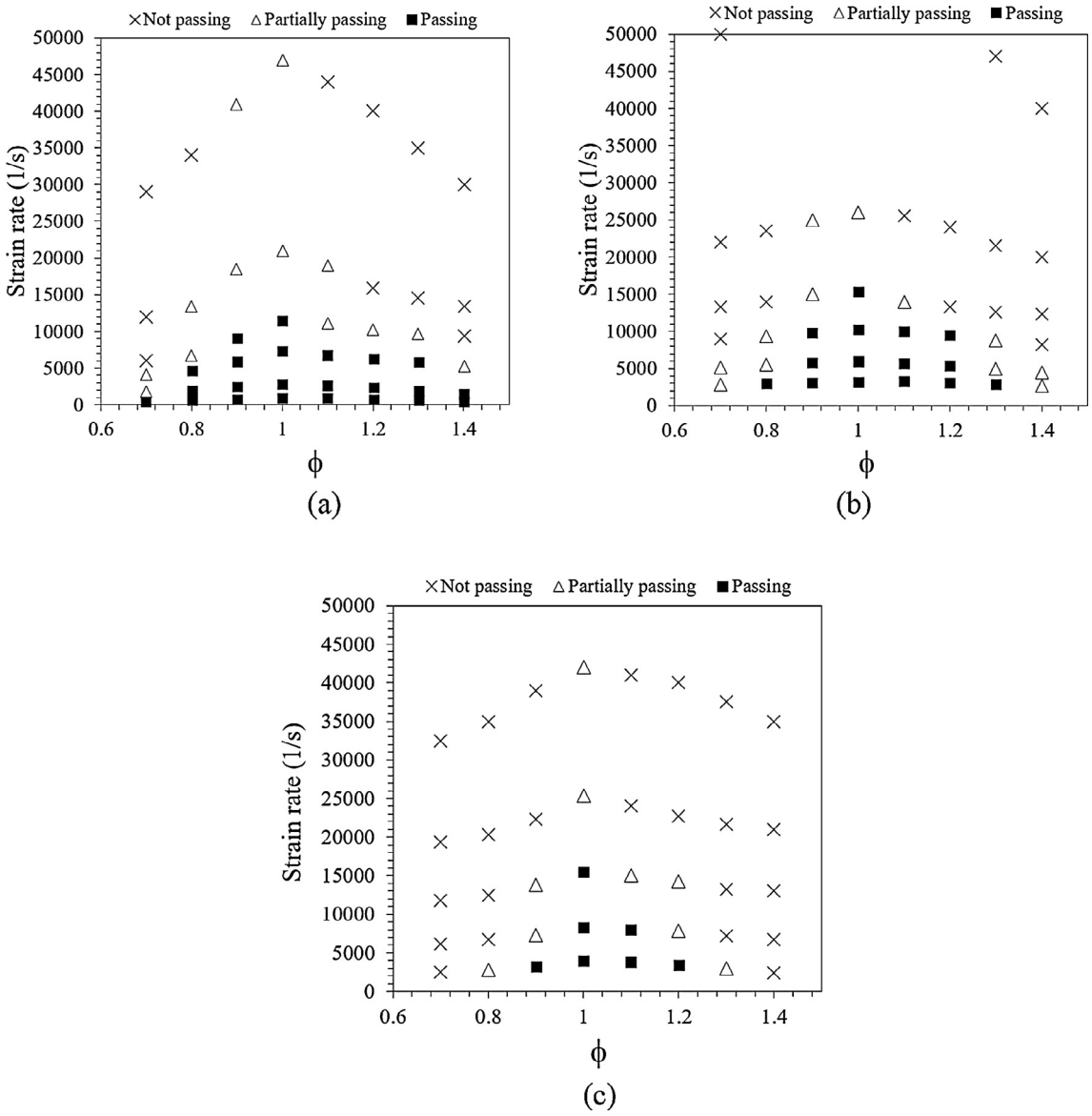

Fig. 14. Strain rate as a function of equivalence ratio for (a) straight channels and (b) C-D channels with AR = 4, (c) C-D channels with AR = 9.

loss reveal that heat loss was the primary reason for the partial passing of flames through the microchannel. The isolated stretch effect was also studied with the heat loss effect fixed. Due to the stretch effect, the critical equivalence ratio in the C-D microchannel was closer to the stoichiometric condition than the straight channel. Lastly, flame oscillations were observed in both experiment and simulations for smaller microchannels.

Acknowledgement

The work was supported by the National Science Foundation with Dr. Song-Charng Kong as the technical monitor.

Appendix A. Supplementary material

Supplementary data associated with this article can be found, in the online version, at https://doi.org/10.1016/j.applthermaleng.2018.07.049.

References

[1] A.C. Fernandez-Pello, Micropower generation using combustion: issues and approaches, Proc. Combust. Inst. 29 (2002) 883–899.
[2] N. Chigier, T. Gemci, Meso and micro scale propulsion concepts for small spacecraft, AIAA J. (2003) 670.
[3] D. Dunn-Rankin, E.M. Leal, D.C. Walther, Personal power systems, Prog. Energy Combust. Sci. 31 (5–6) (2005) 422–465.
[4] N. Abas, A. Kalair, N. Khan, Review of fossil fuels and future energy technologies, Futures 69 (2015) 31–49.
[5] Y. Ju, K. Maruta, Microscale combustion: Technology development and fundamental research, Prog. Energy Combust. Sci. 37 (6) (2011) 669–715.
[6] N. Kim, K. Maruta, A numerical study on propagation of premixed flames in small tubes, Combust. Flame 146 (1–2) (2006) 283–301.
[7] H. Nakamura, A. Fan, S. Minaev, E. Sereshchenko, R. Fursenko, Y. Tsuboi, K. Maruta, Bifurcations and negative propagation speeds of methane/air premixed flames with repetitive extinction and ignition in a heated microchannel, Combust. Flame 159 (4) (2012) 1631–1643.
[8] K. Maruta, Micro and mesoscale combustion, Proc. Combust. Inst. 33 (1) (2011) 125–150.
[9] K. Maruta, T. Kataoka, N.I. Kim, S. Minaev, R. Fursenko, Characteristics of combustion in a narrow channel with a temperature gradient, Proc. Combust. Inst. 30 (2) (2005) 2429–2436.
[10] S. Biswas, L. Qiao, Ignition of ultra-lean premixed H2/air using multiple hot turbulent jets generated by pre-chamber combustion, Appl. Therm. Eng. 132 (5) (2018) 102–114.
[11] S. Biswas, L. Qiao, A numerical investigation of ignition of ultra-lean premixed H2/

air mixtures by pre-chamber supersonic hot jet, SAE Int. J. Engines 10 (5) (2017) 2231–2247.
[12] S. Biswas, S. Tanvir, H. Wang, L. Qiao, On ignition mechanisms of premixed CH4/air and H2/air using a hot turbulent jet generated by pre-chamber combustion, Appl. Therm. Eng. 106 (2016) 925–937.
[13] S. Biswas, L. Qiao, Prechamber hot jet ignition of ultra-lean H2/air mixtures: effect of supersonic jets and combustion instability, SAE Int. J. Engines (2016) 9(3).
[14] S. Biswas, Physics of Turbulent Jet Ignition: Mechanisms and Dynamics of Ultra-lean Combustion, first ed., Springer, 2018.
[15] S. Biswas, L. Qiao, Ignition of ultra-lean premixed hydrogen/air by an impinging hot jet, Appl. Energy 228 (2018) 954–964.
[16] S. Biswas, L. Qiao, Combustion instabilities of ultra-lean premixed H2/air mixtures by pre-chamber turbulent jet ignition, J. Propul. Power (2018).
[17] S. Biswas, L. Qiao, A comprehensive statistical investigation of schlieren image velocimetry (SIV) using high-velocity helium jet, Exp. Fluids 58 (3) (2017) 1–20.
[18] Y. Ju, B. Xu, Theoretical and experimental studies on mesoscale flame propagation and extinction, Proc. Combust. Inst. 30 (2) (2005) 2445–2453.
[19] A. Alipoor, K. Mazaheri, A. Shamooni Pour, Y. Mahmoudi, Asymmetric hydrogen flame in a heated micro-channel: Role of Darrieus-Landau and thermal-diffusive instabilities, Int. J. Hydrogen Energy 41 (44) (2016) 20407–20417.
[20] A. Alipoor, K. Mazaheri, Combustion characteristics and flame bifurcation in repetitive extinction-ignition dynamics for premixed hydrogen-air combustion in a heated micro channel, Energy 109 (2016) 650–663.
[21] Y. Wang, Z. Zhou, W. Yang, J. Zhou, J. Liu, K. Cen, The impact of preheating on stability limits of premixed hydrogen-air combustion in a microcombustor, Heat Transfer Eng. 33 (7) (2012) 661–668.
[22] C.Y.H. Chao, K.S. Hui, W. Kong, P. Cheng, J.H. Wang, Analytical and experimental study of premixed methane–air flame propagation in narrow channels, Int. J. Heat Mass Transf. 50 (7–8) (2007) 1302–1313.
[23] M. Sánchez-Sanz, D. Fernández-Galisteo, V.N. Kurdyumov, Effect of the equivalence ratio, Damköhler number, Lewis number and heat release on the stability of laminar premixed flames in microchannels, Combust. Flame 161 (5) (2014) 1282–1293.
[24] C. Mauger, L. Méès, M. Michard, M. Lance, Velocity measurements based on shadowgraph-like image correlations in a cavitating micro-channel flow, Int. J. Multiph. Flow 58 (2014) 301–312.
[25] J. Li, P. Zhang, L. Yuan, Z. Pan, Y. Zhu, Flame propagation and detonation initiation distance of ethylene/oxygen in narrow gap, Appl. Therm. Eng. 110 (2017) 1274–1282.
[26] J. Li, S.K. Chou, G. Huang, W.M. Yang, Z.W. Li, Study on premixed combustion in cylindrical micro combustors: Transient flame behavior and wall heat flux, Exp. Therm Fluid Sci. 33 (4) (2009) 764–773.
[27] Y. Fan, Y. Suzuki, N. Kasagi, Experimental study of micro-scale premixed flame in quartz channels, Proc. Combust. Inst. 32 (2) (2009) 3083–3090.
[28] W. Yang, C. Deng, J. Zhou, J. Liu, Y. Wang, K. Cen, Experimental and numerical investigations of hydrogen–air premixed combustion in a converging–diverging micro tube, Int. J. Hydrogen Energy 39 (7) (2014) 3469–3476.
[29] S.W. Churchill, H.H.S. Chu, Orrelating equations for laminar and turbulent free convection from a horizontal cylinder, Int. J. Heat Mass Transf. 18 (1975) 1049–1053.
[30] M. Frenklach, H. Wang, M. Goldenberg, G.P. Smith, D.M. Golden, GRI-MECH: An Optimized Detailed Chemical Reaction Mechanism for Methane Combustion, Gas Research Institute, Chicago, 1995.
[31] GRI-Mech 1.2 http://www.me.berkeley.edu/gri_mech/.
[32] S.B. Pope, Computationally efficient implementation of combustion chemistry using in situ adaptive tabulation, Combust. Theor. Model. 1 (1) (1997) 41–63.
[33] K. Maruta, J.K. Parc, K.C. Oh, T. Fujimori, S.S. Minaev, R.V. Fursenko, Characteristics of microscale combustion in a narrow heated channel, Combust., Explosion Shock Waves 40 (5) (2004) 516–523.
[34] T.L. Jackson, J. Buckmaster, Z. Lu, D.C. Kyritsis, L. Massa, Flames in narrow circular tubes, Proc. Combust. Inst. 31 (1) (2007) 955–962.